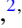# Fate of Majorana zero modes, exact location of critical states, and unconventional real-complex transition in non-Hermitian quasiperiodic lattices

Tong Liu [1,*] Shujie Cheng,[2,†] Hao Guo [3,‡] and Gao Xianlong [2,§]

[1]*Department of Applied Physics, School of Science, Nanjing University of Posts and Telecommunications, Nanjing 210003, China*
[2]*Department of Physics, Zhejiang Normal University, Jinhua 321004, China*
[3]*Department of Physics, Southeast University, Nanjing 211189, China*

We study a one-dimensional p-wave superconductor subject to non-Hermitian quasiperiodic potentials. Although non-Hermiticity exists, the Majorana zero mode is still robust against the disorder perturbation. The analytic topological phase boundary is verified by calculating the energy gap closing point and the topological invariant. Furthermore, we investigate the localized properties of this model, quantitatively revealing that the topological phase transition is accompanied by the Anderson localization phase transition, and a wide critical phase emerges with amplitude increments of the non-Hermitian quasiperiodic potentials. Finally, we numerically uncover a unconventional real-complex transition of the energy spectrum, which is different from the conventional $\mathcal{PT}$ symmetric transition.

I. INTRODUCTION

The discovery of Anderson localization [1] belongs to the very heart in understanding how the disorder affects the mobility of carriers through the spatial distribution of the wave function. After half a century, the Anderson localization phenomena were observed in a ultracold atomic experiment with correlated disordered potentials [2] and incommensurate/quasiperiodic potentials [3]. Nowadays, Anderson localization has been one of the important and highly explored research subjects in condensed matter physics [4–7]. In one-dimensional systems it has been shown that the interplay between particle interactions and random disordered or incommensurate disordered external potentials forms the many-body localization [8–13], a many-body version of Anderson localization.

A paradigm to understand the Anderson localization is the Aubry-André-Harper (AAH) model [14,15], in which the increased strength of the incommensurate potential leads to a localized transition. In some variants of the AAH models, the rich localization phenomena can be observed [16–20]. Another interesting aspect of generalized AAH models is the presence of a mobility edge in energy separating extended from localized states [20–26]. It should be noted that the one-dimensional AAH model can be understood as the projection of the two-dimensional Hofstadter model in the one-dimensional direction [14,27,28], which supports topologically protected edge states localized at the boundary, similar to the edge states in quantum Hall insulators [29,30]. Consequently, the topological properties of one-dimensional quasicrystals have been gradually excavated according to this projection [31–35]. In topological community, the one-dimensional p-wave superconductor chain is another important paradigm [36–39]. A key feature of the one-dimensional p-wave superconductor is that it hosts topologically protected Majorana zero modes (MZMs) [40–43], an ideal platform for the error-free quantum computation due to the immunity to the weakly disordered perturbation of the qubits [44,45]. Thus, the interplay of disorder and topology in one-dimensional quasiperiodic lattices with p-wave superconducting pairing deserves further investigations. Reference [46] uncovered that the topological phase transition is accompanied by the Anderson localization phase transition in a Hermitian quasiperiodic chain with p-wave superconducting pairing. Further research showed that there exists a critical phase in the topologically nontrivial region [28].

Non-Hermitian lattices show exotic physical phenomena without Hermitian counterparts, such as the exceptional points, breakdown of the Bloch bulk-boundary correspondence, and the non-Hermitian skin effect [47–52]. However, a systematical study about the interplay between the quasiperiodic disorder, topology, and non-Hermitian [53–57] is still absent to the best of our knowledge. Here a major question arises: what kind of physical phenomena can be shown in a one-dimensional p-wave superconductor subject to non-Hermitian quasiperiodic potentials? What is the fate of the MZMs and the critical states? Is there real-complex transition in the presence of non-Hermiticity? In this work we are devoted to answer these questions.

II. MODEL AND HAMILTONIAN

We consider the one-dimensional p-wave superconductor subject to non-Hermitian quasiperiodic potentials, described

*t6tong@njupt.edu.cn
†2818917376@qq.com
‡guohao.ph@seu.edu.cn
§gaoxl@zjnu.edu.cn

by

$$\hat{H} = \sum_{n=1}^{L-1}(-t\hat{c}_n^\dagger\hat{c}_{n+1} + \Delta\hat{c}_n\hat{c}_{n+1} + \text{H.c.}) + \sum_{n=1}^{L}V_n\hat{c}_n^\dagger\hat{c}_n, \quad (1)$$

where $\hat{c}_n^\dagger$ ($\hat{c}_n$) is the fermion creation (annihilation) operator, and L is the total number of sites. The nearest-neighbor hopping amplitude t and the p-wave pairing amplitude Δ are real constants, and $V_n = Ve^{i2\pi\alpha n}$ is the non-Hermitian quasiperiodic potential. Specially, the real Δ can be realized by manipulating the interaction strength and the loss rate in a BEC system [58,59]. A typical choice for parameter α is $\alpha = (\sqrt{5}-1)/2$. For computational convenience, $t = 1$ is set as the energy unit. In the topological classification, this model belongs to the D class [60] and it does not preserve $\mathcal{PT}$ symmetry [49]. When Δ is equal to zero, this model reduces to the non-Hermitian AAH model [22], where the localized transition and the topological properties are well understood. When $\alpha = 0$, this Hamiltonian describes the Kitaev model, where there are topologically protected MZMs [38,45]. When the imaginary part of the non-Hermitian potential is omitted, the model reduces to the Hermitian non-Abelian AAH model [28,46], in which the topological phase transition and the Anderson localization transition are well studied.

The Hamiltonian (1) can be diagonalized by using the Bogoliubov–de Gennes (BdG) transformation: $\hat{\chi}_m^\dagger = \sum_{n=1}^{L}[u_{m,n}\hat{c}_n^\dagger + v_{m,n}\hat{c}_n]$, where L denotes the total number of sites, n is the site index, and $u_{m,n}, v_{m,n}$ are the two components of wave functions. It is widely known that the particle-hole symmetry is preserved [38]. Under this transformation, the BdG equations can be expressed as

$$t(u_{n+1} + u_{n-1}) + Ve^{i2\pi\alpha n}u_n - \Delta(v_{n+1} - v_{n-1}) = E_m u_n,$$
$$\Delta(u_{n+1} - u_{n-1}) - Ve^{i2\pi\alpha n}v_n - t(v_{n+1} + v_{n-1}) = E_m v_n. \quad (2)$$

where E_m is the complex eigenenergy, indexed according to its real part $\text{Re}(E_m)$ and arranged in ascending order with m being the energy level index.

By numerically solving Eq. (2), we can obtain the energy spectrum of the system and the components $u_{m,n}$ and $v_{m,n}$ of the wave functions. The inverse participation ratio (IPR) is usually used to study the localization-delocalization transition [14,22,28,46]. For any given normalized wave function, the corresponding IPR is defined as $\text{IPR}_m = \sum_{n=1}^{L}(|u_{m,n}|^4 + |v_{m,n}|^4)$ which measures the inverse of the number of sites being occupied by particles. It is well known that the IPR of an extended state scales like L^{-1} which approaches zero in the thermodynamic limit. However, for a localized state, since only finite number of sites are occupied, the IPR is finite even in the thermodynamic limit. The mean of IPR over all the $2L$ eigenstates is dubbed the MIPR expressed as $\text{MIPR} = \frac{1}{2L}\sum_{m=1}^{2L}\text{IPR}_m$.

III. FATE OF MAJORANA ZERO MODES

In this part we will study the fate of the MZMs and the topological phase transition. The top panel in Fig. 1 shows the real part of the energy spectrum of Eq. (1) as a function of the non-Hermitian potential strength V under the open boundary condition (OBC), with the parameters $\Delta = 0.5$ and
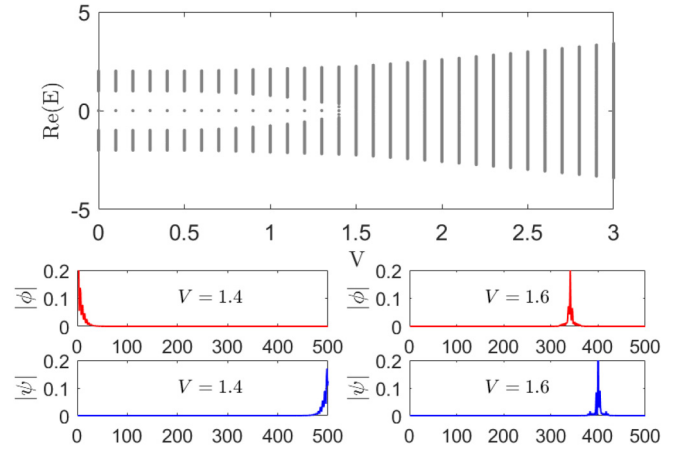

FIG. 1. Top panel: The real part of eigenvalues of Eq. (1) as a function of V under OBC. Definitely there are stable MZMs when $V < t + \Delta$. As the value of V continuously increases, the MZM eventually vanishes, and the phase transition point is roughly located at $V_c = t + \Delta$. Bottom panel: Spatial distributions of ϕ and ψ for the lowest excitation modes with $V = 1.4$ (bottom panel left) and with $V = 1.6$ (bottom panel right). Obviously when $V = 1.4$, ϕ and ψ are symmetrically distributed at the ends of the chain, indicating the topological nontrivial phase, whereas they are located inside of the chain when $V = 1.6$. Other involved parameters are $t = 1$, $\alpha = (\sqrt{5}-1)/2$, $\Delta = 0.5$, and $L = 500$.

$L = 500$. As shown in the figure, there are stable MZMs when $V < t + \Delta$. However, when V is larger than the critical value V_c, MZMs annihilate and then enter into the bulk of the system. Hence, the systems will undergo a topological nontrivial to a trivial phase transition as V increases, and the visible phase transition point is about $V_c = t + \Delta$. Similar to the previous works [28,38,45,46], MZMs in our system are still localized at ends of the system. To understand the Majorana edge state deeply, we introduce the Majorana operators, namely $\lambda_n^A = \hat{c}_n^\dagger + \hat{c}_n$ and $\lambda_n^B = i(\hat{c}_n^\dagger - \hat{c}_n)$, which obey the relations $(\lambda_n^\beta)^\dagger = \lambda_n^\beta$ and $\{\lambda_n^\beta, \lambda_{n'}^{\beta'}\} = 2\delta_{nn'}\delta_{\beta\beta'}$, with β, $\beta' \in \{A, B\}$. Accordingly, in the Majorana picture, the quasiparticle operator $\hat{\chi}_m^\dagger$ can be rewritten as $\hat{\chi}_m^\dagger = \frac{1}{2}\sum_{n=1}^{L}[\phi_{m,n}\lambda_n^A - i\psi_{m,n}\lambda_n^B]$, in which $\phi_{m,n} = (u_{m,n} + v_{m,n})$ and $\psi_{m,n} = (u_{m,n} - v_{m,n})$.

The bottom panel of Fig. 1 plots the spatial distributions of ϕ and ψ for the lowest excitation mode [46,61] under OBC, with $\Delta = 0.5$ and $V = 1.4$ (left bottom panel) and $V = 1.6$ (right bottom panel). When $V = 1.4$, the lowest excitation mode is just the MZM. Our numerical investigations show that there is no anomalous edge state [62] and the skin effect [63,64] and the Majorana edge states ϕ and ψ are localized at the ends of the system. On the contrary, when $V = 1.6$, the lowest excitation mode is no longer the MZM. As a result, the visible distributions of ϕ and ψ in the right bottom panel are located inside the bulk of the system. Therefore, only if V is less than V_c, the system is topologically nontrivial and supports the MZMs.

Due to the bulk-edge correspondence, the topological properties of non-Hermitian systems are generally protected by the real gap [45,65]. We suppose that this correspondence is still applicative for our model. Therefore, we first deduce the
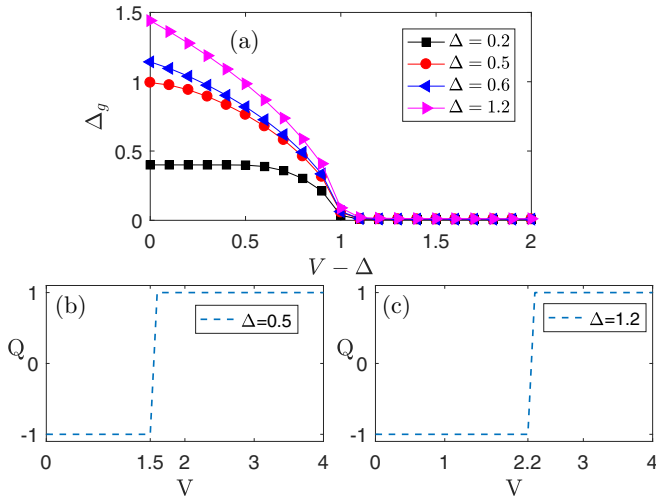
FIG. 2. (a) The real energy gap Δ_g as a function of $V - \Delta$ under PBC. Intuitively, the gap closes at $V_c = t + \Delta$. (b) and (c) The topological invariant Q as a function of V with two chosen Δ. When $V < t + \Delta$, $Q = -1$, corresponding to the topologically nontrivial phase; when $V > t + \Delta$, $Q = 1$, corresponding to the topologically trivial phase. Intuitively, Q jumps at the phase transition point, i.e., the gap-closing point $V_c = t + \Delta$. Other involved parameters are $t = 1$, $\alpha = (\sqrt{5} - 1)/2$, and $L = 500$.

topological phase transition point by calculating the gap-closing point. By the method in Refs. [46,66] we eventually obtain the following constraint condition:

$$\prod_{n=1}^{L} e^{i2\pi\alpha n} = \left(\frac{t + \Delta}{V}\right)^{L}. \tag{3}$$

In the thermodynamic limit $L \to \infty$, V has a real solution if $V = t + \Delta$ (see details in Appendix A), thus, we obtain the gap-closing point $V_c = t + \Delta$.

In order to verify the accuracy of the analytical V_c, and to understand the relationship between the topological phase transition and the gap closing, we numerically plot the variation of the real energy gap Δ_g with respect to the non-Hermitian quasiperiodic potential strength V under PBC, as shown in Fig. 2(a). It is readily seen that the real energy gap closes at $V_c = t + \Delta$ even though the size of the system is finite.

In addition to the mentioned MZM and the gap-closing point, the topological phase transition is more precisely characterized by the topological invariant Q, which can be evaluated by the transfer matrix numerically [67,68] (see details in Appendix B). In Figs. 2(b) and 2(c) we plot the variation of the topological invariant Q versus V for different Δ. When $V < t + \Delta$, $Q = -1$ corresponds to the topologically nontrivial phase; when $V > t + \Delta$, $Q = 1$ corresponds to the topologically trivial phase. Intuitively, Q jumps at the phase transition point, i.e., the gap-closing point $V_c = t + \Delta$. This illustrates that the topological properties of the system are exactly protected by the real gap and the introduced non-Hermiticity compresses the topologically nontrivial region relative to the Hermitian counterpart [46].
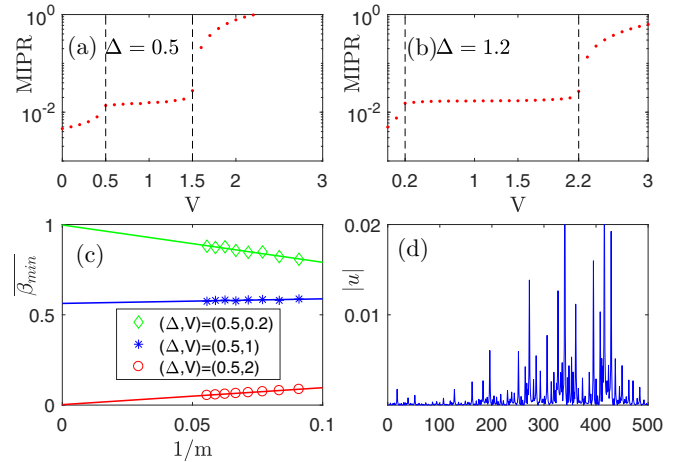

FIG. 3. MIPR as a function of V with (a) $\Delta = 0.5$ and (b) $\Delta = 1.2$. The dashed lines show the sharp increase of the MIPR at phase boundaries $V_{ec} = |t - \Delta|$ and $V_c = t + \Delta$. (c) $\overline{\beta_{\min}}$ as a function of the inverse Fibonacci index $1/m$ at $(\Delta, V) = (0.5, 0.2)$, $(0.5, 1)$, and $(0.5, 2)$. These three points are located in the extended, critical, and localized phases, respectively. (d) The representative wave function is illustrated for the critical phase $(\Delta, V) = (0.5, 1)$ and $L = 500$. Other involved parameters are $t = 1$, $\alpha = (\sqrt{5} - 1)/2$.

IV. EXACT LOCATION OF THE CRITICAL STATES

Recalling the localized distributions of the lowest excitation modes in Fig. 1 when $V > V_c$, we are well aware that there is an Anderson localization phase transition together with the topological phase transition. Figures 3(a) and 3(b) plot the variation of MIPR as a function of the potential strength V with various Δ. Intuitively, the MIPR increases steeply at V_c and approaches 1. Such a phenomenon signals a delocalization-localization phase transition, and the region where $V > V_c$ denotes the Anderson localization phase. However, the region where $V < V_c$ is not necessarily the extended phase. Instead, it is divided into two phases, i.e., the extended phase and the critical one. The MIPR of the critical phase is greater than that of the extended one and less than that of the localized one and forms a platform. The extended-critical phase transition point V_{ec} is readily seen at $V_{ec} = t - \Delta$.

We further validate our analysis by using the fractal dimension $\overline{\beta_{\min}}$ (see details in Appendix C). For localized (extended) states, $\overline{\beta_{\min}} \to 0\,(1)$, whereas $0 < \overline{\beta_{\min}} < 1$ for the critical states. Figure 3(c) shows the $\overline{\beta_{\min}}$ as a function of the inverse Fibonacci index $1/m$ (L is chosen as the mth Fibonacci number F_m) for various parameter points (Δ, V). We find that $\overline{\beta_{\min}}$ tends to 1 at $(\Delta, V) = (0.5, 0.2)$, suggesting that the system is in the extended phase. $\overline{\beta_{\min}}$ extrapolates to 0 at $(\Delta, V) = (0.5, 2)$, indicating that the system is in the localized phase. For $(\Delta, V) = (0.5, 1)$, the corresponding $\overline{\beta_{\min}}$ in the thermodynamic limit is intuitively between 0 and 1, signaling the typical critical wave function in Fig. 3(d). We emphasize that such an analysis strategy works for other parameter points as well. Hence, we verify that there are indeed extended and critical phases in the topologically nontrivial region.

Actually, for the Hermitian quasiperiodic chain with p-wave superconducting pairing, Wang *et al.* [28] also numerically uncover a similar critical region located at
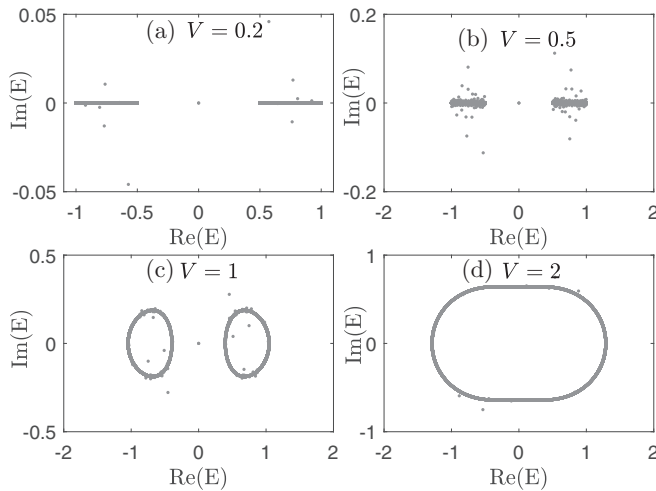
FIG. 4. The eigenenergies of Eq. (1) with $\Delta = 0.5$ and $L = 5000$ under OBC. (a) $V = 0.2$ is taken from the extended and topologically nontrivial phase. The eigenenergies are totally real. (b) $V = 0.5$ is taken at the extended-critical transition point and the imaginary parts of eigenenergies have a certain width. (c) $V = 1$ is taken from the critical phase and the imaginary parts of eigenenergies are completely broadened. (d) $V = 2$ is taken from the localized phase, the imaginary parts of eigenenergies are also completely broadened. Other involved parameters are $t = 1$ and $\alpha = (\sqrt{5} - 1)/2$.

$2(t - \Delta) \leqslant V \leqslant 2(t + \Delta)$. However, it is a long-standing unsolved question to quantitatively explain the location of the critical region. By making use of the transfer matrix method for Majorana zero modes (see details in Appendix D), we analytically demonstrate that when $V > t + \Delta$, the Majorana wave function ψ becomes localized (also regarded as the topological phase transition), while $V > t - \Delta$, the Majorana wave function ϕ becomes localized. Consequently, within the region $V_{ec} \leqslant V \leqslant V_c$, the ensemble of the Majorana wave functions can be regarded as semiextended and semilocalized, i.e., critical. Thus we phenomenologically conclude the emergence of the critical states for the non-Hermitian version of the quasiperiodic p-wave pairing model, which can be directly generalized to the Hermitian counterpart [28].

V. UNCONVENTIONAL REAL-COMPLEX TRANSITION

By analyzing the energy spectrum, we find that there exists the unconventional real-complex transition of energy. The unconventionality has two implications. For one thing, compared to the $\mathcal{PT}$-symmetric systems [22,45,49–58], this transition still exists in our system without $\mathcal{PT}$ symmetry. For another, our finding is very different from what uncovered by Hamazaki *et al.* [69]. The difference lies in three aspects: First, Hamazaki *et al.* found that such a transition occurred when the time reversal symmetry was present, but it appears in our model without time reversal symmetry. Second, the real energy region was located in the localized phase, whereas in our model, it locates in the extended phase. Third, the time reversal symmetry was responsible for the presented real-complex transition, while our model provides an exception.

In Fig. 4 we take $\Delta = 0.5$ and fix the size of the system $L = 5000$ and display the eigenenergies of Eq. (1) with
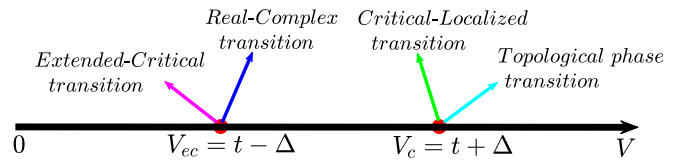

FIG. 5. Phase diagram of the model in this paper. $V_{ec} = t - \Delta$ (the left red dot) is the transition point of the extended-critical transition and the real-complex transition. $V_c = t + \Delta$ (the right red dot) is the transition point of the critical-localized transition and the topological phase transition.

various V under OBC. As the figure shows, when $V = 0.2$, the eigenenergies are real, and the system is in the extended and topologically nontrivial phase. $V = 0.5$ is chosen at the extended-critical transition point. Although the system is still in the topologically nontrivial phase, the imaginary parts of eigenenergies have a certain width. $V = 1$ is in the critical and topologically nontrivial phase, it can be distinctly shown that the eigenenergies of the system are complex. The similar phenomenon also occurs in the case of $V = 2$, in which the system is in the localized and topologically trivial phase. The energy spectra with loop in Figs. 4(c) and 4(d) imply that such a unconventional real-complex transition is independent of the skin effect [70,71]. We have also checked other combinations of parameters and get the same results as expected. Accordingly, we draw another conclusion that only the extended phase support the fully real eigenenergies, thus, provide a new result to explore the rich physics of non-Hermitian systems.

Synthesizing the above analyses, we finally obtain the total phase diagram of the system, shown in Fig. 5. As the diagram shows, the left red dot denotes the extended-critical and the real-complex transition point V_{ec}, satisfying $V_{ec} = t - \Delta$. The right red dot corresponds to the critical-localized and the topological phase transition point V_c, satisfying $V_c = t + \Delta$.

VI. SUMMARY

In summary, we have studied the topological properties and investigated the extended, critical, and localized phases of a one-dimensional p-wave superconductor subject to the non-Hermitian quasiperiodic potentials. By analyzing the energy spectrum, it is shown that there are MZMs protected by the energy gap, and the analytic topological transition point is verified by calculating the energy gap and the topological invariant. Furthermore, we quantitatively demonstrate the exact location of the critical region for the quasiperiodic p-wave pairing model through the transfer matrix method, which solves a long-standing question. More impressively, for our system without $\mathcal{PT}$ symmetry, we find an unconventional real-complex transition of the eigenenergies and the energies in the extended phase are fully real. Our finding may form a new universality class about the real-complex transition. Unfortunately we have failed to obtain an analytical expression of the real-complex transition point. However, it remains an open question to explore the relationship between the extended phase and the real energy, even if there is no $\mathcal{PT}$ symmetry.

APPENDIX A: DERIVATION OF THE GAP-CLOSING POINT V_c

Under the periodic boundary condition (PBC), the Hamiltonian in Eq. (1) can be rewritten as

$$\hat{H} = \sum_{nn'}\left[\hat{c}_n^\dagger M_{nn'}\hat{c}_{n'} + \frac{1}{2}(\hat{c}_n^\dagger N_{nn'}\hat{c}_{n'}^\dagger + \text{H.c.})\right], \quad \text{(A1)}$$

where M is a Hermitian matrix and N is an antisymmetric matrix, respectively expressed as

$$M = \begin{pmatrix} V_1 & -t & \cdots & -t \\ -t & V_2 & & \\ \vdots & & \ddots & -t \\ -t & & -t & V_L \end{pmatrix}, \quad N = \begin{pmatrix} 0 & -\Delta & \cdots & \Delta \\ \Delta & 0 & & \\ \vdots & & \ddots & -\Delta \\ -\Delta & & \Delta & 0 \end{pmatrix}. \quad \text{(A2)}$$

With the above matrices we can determine the excitation spectrum E_m via solving the secular equation

$$\det\left[(M+N)(M-N) - E_m^2\right] = 0. \quad \text{(A3)}$$

Accordingly, the transition point V_c can be solved by the equation $\det[(M+N)(M-N)] = 0$. Having known that $\det(M-N) = \det(M-N)^T = \det(M+N)$, then V_c is further determined by $\det(M-N) = 0$. Eventually we obtain the following constraint condition:

$$\prod_{n=1}^{L} e^{i2\pi\alpha n} = \left(\frac{t+\Delta}{V}\right)^L. \quad \text{(A4)}$$

In the thermodynamic limit $L \to \infty$, V_c has a real solution, and $V_c = t + \Delta$.

APPENDIX B: TRANSFER MATRIX METHOD FOR TOPOLOGICAL INVARIANT Q

In this Appendix we introduce the transfer matrix method to derive the topological invariant Q. In a p-wave superconducting wire, the topological phase transition is characterized by the change of the topological quantum number Q. The value of $Q = (-1)^m$ is determined by the parity of the number m of Majorana bound states at each end of the wire, and $Q = -1$ denotes the topological phase. The scattering matrix $\mathcal{S}$ is defined to relate the incoming and outgoing wave amplitudes. In the disordered p-wave superconducting wire, the waves can come in from the left/right end of the chain in two channels, i.e., particle and hole channels, so $\mathcal{S}$ is a 4×4 unitary matrix. The 2×2 subblocks R, R' and T, T' are defined as the reflection and transmission matrices at two ends of the chain, respectively,

$$\mathcal{S} = \begin{pmatrix} R & T' \\ T & R' \end{pmatrix}, \quad \text{(B1)}$$

where

$$R = \begin{pmatrix} r_{ee} & r_{eh} \\ r_{he} & r_{hh} \end{pmatrix}. \quad \text{(B2)}$$

Here r_{ee} and r_{eh} are the normal and Andreev reflection amplitudes, respectively. Note the BdG Hamiltonian of the system has a particle-hole symmetry

$$\mathcal{P}H_{\text{BdG}}\mathcal{P}^{-1} = -H_{\text{BdG}}, \quad \text{(B3)}$$

where $\mathcal{P} = \tau_x C$ with τ_x being the first Pauli matrix and C being the complex conjugation operator. This leads to the following constraint on the reflection matrix:

$$\tau_x R \tau_x = R^*, \quad \text{(B4)}$$

which implies

$$\det(R) = \det(R)^*. \quad \text{(B5)}$$

Here we have implicitly applied the condition that the Fermi level $E = 0$. At the Fermi level the transmission T through the superconducting wire is 0 because there are no extended states from one end to the other. Therefore the reflection matrix R is unitary, i.e., $RR^\dagger = 1$, which implies

$$|\det(R)| = 1. \quad \text{(B6)}$$

Combining with the condition (B5), we get $\det(R) = \pm 1$. Consequently the topological quantum number is $Q = \text{sgn}[\det(R)]$.

In the practical numerical calculation, the scattering matrix can be obtained by the transfer matrix scheme

$$\begin{pmatrix} \hat{t}_i\Phi_i \\ \Phi_{i+1} \end{pmatrix} = M_i\begin{pmatrix} \hat{t}_{i-1}^\dagger\Phi_{i-1} \\ \Phi_i \end{pmatrix}, \quad \text{(B7a)}$$

$$M_i = \begin{pmatrix} 0 & \hat{t}_i^\dagger \\ -\hat{t}_i^{-1} & -\hat{t}_i^{-1}\hat{h}_i \end{pmatrix}, \quad \text{(B7b)}$$

where $\Phi_i = (\phi_i, \psi_i)^T$ is the two-component wave functions on site i. Waves at the two ends of the chain are related by the total transfer matrix

$$M = M_L M_{L-1} \cdots M_2 M_1. \quad \text{(B8)}$$

Next, we transform to a new basis with right-moving and left-moving waves separated in the upper and lower two components by means of the unitary transformation

$$\tilde{M} = U^\dagger M U, \quad U = \sqrt{\frac{1}{2}}\begin{pmatrix} 1 & 1 \\ iI & -iI \end{pmatrix}. \quad \text{(B9)}$$

Under this basis the transmission and reflection matrices are related by

$$\begin{pmatrix} T \\ 0 \end{pmatrix} = \tilde{M}\begin{pmatrix} I \\ R \end{pmatrix}, \quad \begin{pmatrix} R' \\ I \end{pmatrix} = \tilde{M}\begin{pmatrix} 0 \\ T' \end{pmatrix}. \quad \text{(B10)}$$

Finally, the topological invariant Q is evaluated by calculating the *transfer matrix* $\tilde{M}$.

APPENDIX C: DEFINITION OF THE FRACTAL DIMENSION $\overline{\beta_{\text{min}}}$

The fractal theory has been widely applied in the quasiperiodic models [28,61,72–75]. The size of the system L is chosen as the jth Fibonacci number F_j. The advantage of

this arrangement is that the golden ratio can be approximately replaced by the ratio of the nearest two Fibonacci numbers, i.e., $\alpha = (\sqrt{5} - 1)/2 = \lim_{j \to \infty} F_{j-1}/F_j$. Then a scaling index $\beta_{m,n}$ can be extracted from the on-site probability $P_{m,n} = u_{m,n}^2 + v_{m,n}^2$ by

$$P_{m,n} \sim (1/F_j)^{\beta_{m,n}}. \tag{C1}$$

As the fractal theorem tells, when the wave functions are extended, the maximum of $P_{m,n}$ scales as $\max(P_{m,n}) \sim (1/F_j)^1$, implying $\beta_{\min} = 1$. On the other hand, when wave functions are localized, $P_{m,n}$ peaks at very few sites and nearly zero at the others, suggesting $\max(P_{m,n}) \sim (1/F_j)^0$ and $\beta_{\min} = 0$. As for the critical wave functions, the corresponding $\beta_{\min}$ is located within the interval $(0, 1)$. For our system with $L = F_j$ sites, there are $2F_j$ eigenstates. Therefore we can distinguish the extended, the critical, and the localized wave functions by the average of $\beta_{\min}$ (denoted by $\overline{\beta_{\min}}$) over all the eigenstates, and $\overline{\beta_{\min}}$ is expressed as

$$\overline{\beta_{\min}} = \frac{1}{2L} \sum_{m=1}^{2L} \beta_{\min}^m. \tag{C2}$$

APPENDIX D: DERIVATION OF V_{ec} AND V_c BY TRANSFER MATRIX METHOD

In this Appendix we introduce the transfer matrix method which is used to derive the extended-critical transition point $V_{ec} = t - \Delta$ and the critical-localized transition point $V_c = t + \Delta$. Under the Majorana representation, the BdG equation of Hamiltonian can be rewritten in terms of Majorana fermions as

$$(t + \Delta)\psi_{j+1} + (t - \Delta)\psi_{j-1} - V_j \psi_n = E\phi_j,$$
$$(t + \Delta)\phi_{j-1} + (t - \Delta)\phi_{j+1} - V_j \phi_n = E\psi_j. \tag{D1}$$

For Majorana zero modes we only need to focus on the $E = 0$ case and thus two equations above are decoupled and can be reorganized into the transfer matrix form as

$$\begin{pmatrix} \psi_{j+1} \\ \psi_j \end{pmatrix} = T_j \begin{pmatrix} \psi_j \\ \psi_{j-1} \end{pmatrix}, \quad \text{where } T_j = \begin{pmatrix} \frac{V_j}{t+\Delta} & -\frac{t-\Delta}{t+\Delta} \\ 1 & 0 \end{pmatrix}, \tag{D2}$$

$$\begin{pmatrix} \phi_{j+1} \\ \phi_j \end{pmatrix} = T_j' \begin{pmatrix} \phi_j \\ \phi_{j-1} \end{pmatrix}, \quad \text{where } T_j' = \begin{pmatrix} \frac{V_j}{t-\Delta} & -\frac{t+\Delta}{t-\Delta} \\ 1 & 0 \end{pmatrix}. \tag{D3}$$

The transfer matrix method can be used to determine the Anderson localization properties of the normal disordered system. First, we focus on the nature of the Majorana wave function ψ. To transform the disordered p-wave superconducting model to the normal disordered model, we can perform a similarity transformation to the transfer matrix Eq. (D2) as $T_j = \sqrt{\xi} S \tilde{T}_j S^{-1}$ with $S = \text{diag}(\xi^{1/4}, 1/\xi^{1/4})$ and $\xi = \frac{t-\Delta}{t+\Delta}$. Notice that we have set $0 < \Delta < t$. The transfer matrix $\tilde{T}_j$ is

$$\tilde{T}_j = \begin{pmatrix} \frac{V_j}{\sqrt{t^2 - \Delta^2}} & -1 \\ 1 & 0 \end{pmatrix}. \tag{D4}$$

Thus, the total transfer matrix $T \equiv \Pi_{j=1}^L T_j$ becomes

$$T(V, \Delta) = \left(\sqrt{\frac{t-\Delta}{t+\Delta}} \right)^L S \tilde{T} S^{-1}. \tag{D5}$$

We can define the Lyapunov exponent as

$$\gamma = \lim_{L \to \infty} \frac{1}{L} \ln \|T\|. \tag{D6}$$

Combining Eqs. (D5) and (D6) we obtain

$$\gamma(V, \Delta) = \gamma\left(\frac{V}{\sqrt{t^2 - \Delta^2}}, 0 \right) + \ln\left(\sqrt{\frac{t-\Delta}{t+\Delta}} \right). \tag{D7}$$

When $\Delta = 0$, the model is reduced to the non-Hermitian AAH model [22] and the Lyapunov exponent $\gamma(V, 0) = \ln(V)$. The Lyapunov exponent γ is related to the localization length ξ by $\gamma = 1/\xi$. When $\gamma(V, \Delta) = 0$, there is a delocalization-localization transition regarding the Majorana wave function ψ. Substituting $\gamma(\frac{V}{\sqrt{t^2 - \Delta^2}}, 0) = \ln(\frac{V}{\sqrt{t^2 - \Delta^2}})$ into Eq. (D7) and let Eq. (D7) = 0, we can obtain the localization phase transition point $V_c = t + \Delta$, which means when $V > t + \Delta$, the Majorana wave function ψ becomes localized. Equation (D7) is also used to predict the topologically phase transition V_c in the quasiperiodic lattice in the presence of the p-wave pairing.

Similarly, regarding the Majorana wave function ϕ, we can perform a similarity transformation to the transfer matrix Eq. (D3) as $T_j' = \sqrt{\xi'} S' \tilde{T}'_j S'^{-1}$ with $S' = \text{diag}(\xi'^{1/4}, 1/\xi'^{1/4})$ and $\xi' = \frac{t+\Delta}{t-\Delta}$, where $\tilde{T}'_j = \tilde{T}_j$. Thus we obtain the Lyapunov exponent

$$\gamma'(V, \Delta) = \gamma\left(\frac{V}{\sqrt{t^2 - \Delta^2}}, 0 \right) + \ln\left(\sqrt{\frac{t+\Delta}{t-\Delta}} \right). \tag{D8}$$

Therefore we can obtain the delocalization-localization transition point $V_{ec} = t - \Delta$ by setting Eq. (D8) = 0, which means when $V > t - \Delta$, the Majorana wave function ϕ becomes localized.

[1] P. W. Anderson, Absence of diffusion in certain random lattices, Phys. Rev. **109**, 1492 (1958).

[2] J. Billy, V. Josse, Z. Zuo, A. Bernard, B. Hambrecht, P. Lugan, D. Clément, L. Sanchez-Palencia, P. Bouyer, and A. Aspect, Direct observation of Anderson localization of matter waves in a controlled disorder, Nature (London) **453**, 891 (2008).

[3] G. Roati, C. D. Errico, L. Fallani, M. Fattori, C. Fort, M. Zaccanti, G. Modugno, M. Modugno, and M. Inguscio, Anderson localization of a non-interacting Bose-Einstein condensate, Nature (London) **453**, 895 (2008).

[4] A. Pal and D. A. Huse, Many-body localization phase transition, Phys. Rev. B **82**, 174411 (2010).

[5] R. Nandkishore and D. A. Huse, Many-body localization and thermalization in quantum statistical mechanics, Annu. Rev. Comdens. Matter Phys. **6**, 15 (2015).

[6] R. Vosk, D. A. Huse, and E. Altman, Theory of the Many-Body Localization Transition in One-Dimensional Systems, Phys. Rev. X **5**, 031032 (2015).

[7] X. Li, S. Ganeshan, J. H. Pixley, and S. D. Sarma, Many-Body Localization and Quantum Nonergodicit in a Model with a Single-Particle Mobility Edge, Phys. Rev. Lett. **115**, 186601 (2015).

[8] M. Schreiber, S. S. Hodgman, P. Bordia, H. P. Lüschen, M. H. Fischer, R. Vosk, E. Altman, U. Schneider, and I. Bloch, Observation of many-body localization of interacting fermions in a quasirandom optical lattice, Science **349**, 842 (2015).

[9] H. P. Lüschen, P. Bordia, S. Scherg, F. Alet, E. Altman, U. Schneider, and I. Bloch, Observation of Slow Dynamics Near the Many-Body Localization Transition in One-Dimensional Quasiperiodic Systems, Phys. Rev. Lett. **119**, 260401 (2017).

[10] T. Kohlert, S. Scherg, X. Li, H. P. Lüschen, S. D. Sarma, I. Bloch, and M. Aidelsburger, Observation Many-Body Localization in a One-Dimensional System with a Single-Particle Mobility Edge, Phys. Rev. Lett. **122**, 170403 (2019).

[11] H. Yao, H. Khouldi, L. Bresque, and L. Sanchez-Palencia, Critical Behavior and Fractality in Shallow One-Dimensional Quasi-Periodic Potentials, Phys. Rev. Lett. **123**, 070405 (2019).

[12] H. Yao, T. Giamarchi, and L. Sanchez-Palencia, Lieb-Liniger Bosons in a Shallow Quasiperiodic Potential: Bose Glass Phase and Fractal Mott Lobes, Phys. Rev. Lett. **125**, 060401 (2020).

[13] D. A. Abanin, E. Altman, I. Bloch, and M. Serbyn, Colloquium: Many-body localization, thermalization, and entanglement, Rev. Mod. Phys. **91**, 021001 (2019).

[14] S. Aubry and G. André, Analyticity breaking and Anderson localization in incommensurate lattices, Ann. Isr. Phys. Soc. **3**, 133 (1980).

[15] P. G. Harper, The general motion of conduction electrons in a uniform magnetic field, with application to the diamagnetism of metals, Proc. Phys. Soc. London Sect. A **68**, 874 (1955).

[16] S. Das Sarma, S. He, and X. C. Xie, Mobility Edge in a Model One-Dimensional Potential, Phys. Rev. Lett. **61**, 2144 (1988).

[17] D. J. Thouless, Localization by a Potential with Slowly Varying Period, Phys. Rev. Lett. **61**, 2141 (1988).

[18] S. Das Sarma, S. He, and X. C. Xie, Localization, mobility edges, and metal-insulator transition in a class of one-dimensional slowly varying deterministic potentials, Phys. Rev. B **41**, 5544 (1990).

[19] J. Biddle, B. Wang, D. J. Priour, and S. Das Sarma, Localization in one-dimensional incommensurate lattices beyond the Aubry-André model, Phys. Rev. A **80**, 021603(R) (2009).

[20] J. Biddle and S. Das Sarma, Predicted Mobility Edges in One-Dimensional Incommensurate Optical Lattices: An Exactly Solvable Model of Anderson Localization, Phys. Rev. Lett. **104**, 070601 (2010).

[21] J. Biddle, D. J. Priour, B. Wang, and S. Das Sarma, Localization in one-dimensional lattices with non-nearest-neighbor hopping: Generalized Anderson and Aubry-André models, Phys. Rev. B **83**, 075105 (2011).

[22] T. Liu, H. Guo, Y. Pu, and S. Longhi, Generalized Aubry-André self-duality and mobility edges in non-Hermitian quasiperiodic lattices, Phys. Rev. B **102**, 024205 (2020).

[23] H. P. Luschen, S. Scherg, T. Kohlert, M. Schreiber, P. Bordia, X. Li, S. Das Sarma, and I. Bloch, Single-Particle Mobility Edge in a One-Dimensional Quasiperiodic Optical Lattice, Phys. Rev. Lett. **120**, 160404 (2018).

[24] T. Liu and H. Guo, Novel mobility edges in the off-diagonal disordered tight-binding models, Phys. Rev. B **98**, 104201 (2018).

[25] Z. Xu, H. Huangfu, Y. Zhang, and S. Chen, Dynamical observation of mobility edges in one-dimensional incommensurate optical lattice, New J. Phys. **22**, 013036 (2020).

[26] X. Li and S. Das Sarma, Mobility edge and intermediate phase in one-dimensional incommensurate lattice potentials, Phys. Rev. B **101**, 064203 (2020).

[27] D. R. Hofstadter, Energy levels and wave functions of Bloch electrons in rational and irrational magnetic fields, Phys. Rev. B **14**, 2239 (1976).

[28] J. Wang, X.-J. Liu, G. Xianlong, and H. Hu, Phase diagram of a non-Abelian Aubry-André-Harper model with *p*-wave superfluidity, Phys. Rev. B **93**, 104504 (2016).

[29] D. J. Thouless, M. Kohmoto, M. P. Nightingale, and M. den. Nijs, Quantized Hall Conductance in a Two-Dimensional Periodic Potential, Phys. Rev. Lett. **49**, 405 (1982).

[30] Y. Hatsugai, Chern Number and Edge States in the Integer Quantum Hall Effect, Phys. Rev. Lett. **71**, 3697 (1993).

[31] Y. E. Kraus, Y. Lahini, Z. Ringel, M. Verbin, and O. Zilberberg, Topological States and Adiabatic Pumping in Quasicrystals, Phys. Rev. Lett. **109**, 106402 (2012).

[32] Y. E. Kraus and O. Zilberberg, Topological Equivalence between the Fibonacci Quasicrystal and the Harper Model, Phys. Rev. Lett. **109**, 116404 (2012).

[33] L.-J. Lang, X. Cai, and S. Chen, Edge States and Topological Phases in One-Dimensional Optical Superlattices, Phys. Rev. Lett. **108**, 220401 (2012).

[34] L.-J. Lang and S. Chen, Majorana fermions in density-modulated *p*-wave superconducting wires, Phys. Rev. B **86**, 205135 (2012).

[35] S. Ganeshan, K. Sun, and S. Das Sarma, Topological Zero-Energy Modes in Gapless Commensurate Aubry-André-Harper Models, Phys. Rev. Lett. **110**, 180403 (2013).

[36] M. Z Hassan and C. L. Kane, Colloquium: Topological insulators, Rev. Mod. Phys. **82**, 3045 (2010).

[37] X. L. Qi and S.-C. Zhang, Topological insulators and superconductors, Rev. Mod. Phys. **83**, 1057 (2011).

[38] A. Y. Kitaev, Unpaired Majorana fermions in quantum wires, Phys. Usp. **44**, 131 (2001).

[39] D. A. Ivanov, Non-Abelian Statistics of Half-Quantum Vortices in *p*-wave Superconductors, Phys. Rev. Lett. **86**, 268 (2001).

[40] M. Stone and S.-B. Chung, Fusion rules and vortices in $p_x + ip_y$ superconductors, Phys. Rev. B **73**, 014505 (2006).

[41] L. Fu and C. L. Kane, Superconducting Proximity Effect and Majorana Fermions at the Surface of a Topological Insulator, Phys. Rev. Lett. **100**, 096407 (2008).

[42] R. M. Lutchyn, J. D. Sau, and S. Das Sarma, Majorana Fermions and a Topological Phase Transition in Semiconductor-Superconductor Heterostructures, Phys. Rev. Lett. **105**, 077001 (2010).

[43] J. Avila, F. Peñaranda, E. Prada, P. San-Jose, and R. Aguado, Non-Hermitian topology as a unifying framework for the Andreev versus Majorana states controversy, Commun. Phys. **2**, 133 (2019).

[44] A. C. Potter and P. A. Lee, Multichannel Generalization of Kitaev's Majorana End States and a Practical Route to Realize Them in Thin Films, Phys. Rev. Lett. **105**, 227003 (2010).

[45] H. Menke and M. M. Hirschmann, Topological quantum wires with balanced gain and loss, Phys. Rev. B **95**, 174506 (2017).

[46] X. Cai, L.-J. Lang, S. Chen, and Y. Wang, Topological Superconductor to Anderson Localization Transition in One-Dimensional Incommensurate Lattices, Phys. Rev. Lett. **110**, 176403 (2013).

[47] S. Longhi, Topological Phase Transition in Non-Hermitian Quasicrystals, Phys. Rev. Lett. **122**, 237601 (2019).

[48] S. Longhi, Metal-insulator phase transition in a non-Hermitian Aubry-André-Harper Model, Phys. Rev. B **100**, 125157 (2019).

[49] C. M. Bender and S. Boettcher, Real Spectra in Non-Hermitian Hamiltonians having PT Symmetry, Phys. Rev. Lett. **80**, 5243 (1998).

[50] B. Zhu, R. Lü, and S. Chen, PT symmetry in the non-Hermitian Su-Schrieffer-Heeger model with complex boundary potentials, Phys. Rev. A **89**, 062102 (2014).

[51] C. Yuce, Topological phase in a non-Hermitian PT symmetric system, Phys. Lett. A **379**, 1213 (2015).

[52] Y. Liu, X.-P. Jiang, J. Cao, and S. Chen, Non-Hermitian mobility edges in one-dimensional quasicrystals with parity-time symmetry, Phys. Rev. B **101**, 174205 (2020).

[53] L.-Z. Tang, L.-F. Zhang, G.-Q. Zhang, and D.-W. Zhang, Topological Anderson insulators in two-dimensional non-Hermitian disordered systems, Phys. Rev. A **101**, 063612 (2020).

[54] D.-W. Zhang, L.-Z. Tang, L.-J. Lang, H. Yan, and S.-L. Zhu, Non-Hermitian topological Anderson insulators, Sci. China-Phys. Mech. Astron. **63**, 267062 (2020).

[55] W. Gou, T. Chen, D. Xie, T. Xiao, T.-S. Deng, B. Gadway, W. Yi, and B. Yan, Tunable Nonreciprocal Quantum Transport through a Dissipative Aharonov-Bohm Ring in Ultracold Atoms, Phys. Rev. Lett. **124**, 070402 (2020).

[56] F. Alex An, E. J. Meier, and B. Gadway, Engineering a Flux-Dependent Mobility Edge in Disordered Zigzag Chains, Phys. Rev. X **8**, 031045 (2018).

[57] D. S. Borgnia, A. J. Kruchkov, and R.-J. Slager, Non-Hermitian Boundary Modes and Topology, Phys. Rev. Lett. **124**, 056802 (2020).

[58] K. Yamamoto, M. Nakagawa, K. Adachi, K. Takasan, M. Ueda, and N. Kawakami, Theory of Non-Hermitian Fermionic Superfluidity with a Complex-Valued Interaction, Phys. Rev. Lett. **123**, 123601 (2019).

[59] P. San-Jose, E. Cayao, E. Prada, and R. Aguado, Majorana bound states from exceptional points in non-topological superconductors, Sci. Rep. **6**, 21427 (2016).

[60] C.-K. Chiu, J. C. Y. Teo, A. P. Schnyder, and S. Ryu, Classification of topological quantum matter with symmetries, Rev. Mod. Phys. **88**, 035005 (2016).

[61] T. Liu, H.-Y. Yan, and H. Guo, Fate of topological states and mobility edges in one-dimensional slowly varying incommensurate potentials, Phys. Rev. B **96**, 174207 (2017).

[62] T. E. Lee, Anomalous Edge State in a Non-Hermitian Lattice, Phys. Rev. Lett. **116**, 133903 (2016).

[63] S. Yao and Z. Wang, Edge States and Topological Invariants of Non-Hermitian Systems, Phys. Rev. Lett. **121**, 086803 (2018).

[64] F. K. Kunst, E. Edvardsson, J. C. Budich, and E. J. Bergholtz, Biorthogonal Bulk-Boundary Correspondence in Non-Hermitian Systems, Phys. Rev. Lett. **121**, 026808 (2018).

[65] K. Esaki, M. Sato, K. Hasebe, and M. Kohmoto, Edge states and topological phases in non-Hermitian systems, Phys. Rev. B **84**, 205128 (2011).

[66] E. Lieb, T. Schultz, and D. Mattis, Two soluble models of an antiferromagnetic chain, Ann. Phys. (NY) **16**, 407 (1961).

[67] I. Snyman, J. Tworzydlo, and C. W. J. Beenakker, Calculation of the conductance of a graphene sheet using the Chalker-Coddington network model, Phys. Rev. B **78**, 045118 (2008).

[68] P. Zhang and F. Nori, Majorana bound states in a disordered quantum dot chain, New J. Phys. **18**, 043033 (2016).

[69] R. Hamazaki, K. Kawabata, and M. Ueda, Non-Hermitian Many-Body Localization, Phys. Rev. Lett. **123**, 090603 (2019).

[70] N. Okuma, K. Kawabata, K. Shiozaki, and M. Sato, Topological Origin of Non-Hermitian Skin Effects, Phys. Rev. Lett. **124**, 086801 (2020).

[71] K. Zhang, Z. Yang, and C. Fang, Correspondence between Winding Numbers and Skin Modes in Non-Hermitian Systems, Phys. Rev. Lett. **125**, 126402 (2020).

[72] M. Kohmoto and D. Tobe, Localization problem in a quasiperiodic system with spin-orbit interaction, Phys. Rev. B **77**, 134204 (2008).

[73] H. Hiramoto and M. Kohmoto, Scaling analysis of quasiperiodic systems: Generalized Harper model, Phys. Rev. B **40**, 8225 (1989).

[74] Y. Wang, Y. Wang, and S. Chen, Spectral statistics, finite-size scaling and multifractal analysis of quasiperiodic chain with p-wave pairing, Eur. Phys. J. B **89**, 254 (2016).

[75] T. Liu, P. Wang, S. Chen, and G. Xianlong, Phase diagram of a generalized off-diagonal Aubry-André model with p-wave pairing, J. Phys. B **51**, 025301 (2017).